



# Simultaneous excitation of extremely high-Q-factor trapped and octupolar modes in terahertz metamaterials

SHENGYAN YANG,<sup>1,2</sup> CHENGCHUN TANG,<sup>1</sup> ZHE LIU,<sup>1</sup> BO WANG,<sup>1,2</sup> CHUN WANG,<sup>1,2</sup> JUNJIE LI,<sup>1,2,4</sup> LI WANG,<sup>1</sup> AND CHANGZHI GU<sup>1,2,3,5</sup>

<sup>1</sup>Beijing National Laboratory for Condensed Matter Physics, Institute of Physics, Chinese Academy of Sciences, Beijing 100190, China

<sup>2</sup>School of Physical Sciences, CAS Key Laboratory of Vacuum Physics, University of Chinese Academy of Sciences, Beijing 100049, China

<sup>3</sup>Collaborative Innovation Center of Quantum Matter, Beijing, China

<sup>4</sup>jjli@iphy.ac.cn

<sup>5</sup>czgu@iphy.ac.cn

**Abstract:** Achieving high-Q-factor resonances allows dramatic enhancement of performance of many plasmonic devices. However, the excitation of high-Q-factor resonance, especially multiple high-Q-factor resonances, has been a big challenge in traditional metamaterials due to the ohmic and radiation losses. Here, we experimentally demonstrate simultaneous excitation of double extremely sharp resonances in a terahertz metamaterial composed of mirror-symmetric-broken double split ring resonators (MBDSRRs). In a regular mirror-arranged SRR array, only the low-Q-factor dipole resonance can be excited with the external electric field perpendicular to the SRR gap. Breaking the mirror-symmetry of the metamaterial leads to the occurrence of two distinct otherwise inaccessible ultrahigh-Q-factor modes, which consists of one trapped mode in addition to an octupolar mode. By tuning the asymmetry parameter, the Q factor of the trapped mode can be linearly modulated, while the Q factor of the octupolar mode can be tailored exponentially. For specific degree of asymmetry, our simulations revealed a significantly high Q factor ( $Q > 100$ ) for the octupolar mode, which is more than one order of magnitude larger than that of conventional metamaterials. The mirror-symmetry-broken metamaterial offers the advantage of enabling access to two distinct high-Q-factor resonances which could be exploited for ultrasensitive sensors, multiband filters, and slow light devices.

© 2017 Optical Society of America

**OCIS codes:** (160.3918) Metamaterials; (300.6495) Spectroscopy, terahertz; (260.5740) Resonance; (240.0240) Optics at surfaces.

## References and links

1. R. A. Shelby, D. R. Smith, and S. Schultz, "Experimental verification of a negative index of refraction," *Science* **292**(5514), 77–79 (2001).
2. J. Valentine, S. Zhang, T. Zentgraf, E. Ulin-Avila, D. A. Genov, G. Bartal, and X. Zhang, "Three-dimensional optical metamaterial with a negative refractive index," *Nature* **455**(7211), 376–379 (2008).
3. D. Schurig, J. J. Mock, B. J. Justice, S. A. Cummer, J. B. Pendry, A. F. Starr, and D. R. Smith, "Metamaterial electromagnetic cloak at microwave frequencies," *Science* **314**(5801), 977–980 (2006).
4. M. Khorasaninejad, W. T. Chen, R. C. Devlin, J. Oh, A. Y. Zhu, and F. Capasso, "Metalenses at visible wavelengths: diffraction-limited focusing and subwavelength resolution imaging," *Science* **352**(6290), 1190–1194 (2016).
5. S. Zhang, J. Zhou, Y.-S. Park, J. Rho, R. Singh, S. Nam, A. K. Azad, H.-T. Chen, X. Yin, A. J. Taylor, and X. Zhang, "Photoinduced handedness switching in terahertz chiral metamolecules," *Nat. Commun.* **3**, 942 (2012).
6. K. M. Dani, Z. Ku, P. C. Upadhyaya, R. P. Prasankumar, S. R. J. Brueck, and A. J. Taylor, "Subpicosecond optical switching with a negative index metamaterial," *Nano Lett.* **9**(10), 3565–3569 (2009).
7. A. Bitzer, J. Wallauer, H. Helm, H. Merbold, T. Feurer, and M. Walther, "Highly selective terahertz bandpass filters based on trapped mode excitation," *Opt. Express* **17**, 22108–22113 (2009).
8. N. I. Zheludev, E. Plum, and V. A. Fedotov, "Metamaterial polarization spectral filter: isolated transmission line at any prescribed wavelength," *Appl. Phys. Lett.* **99**(17), 171915 (2011).

9. R. Singh, W. Cao, I. Al-Naib, L. Cong, W. Withayachumnankul, and W. Zhang, "Ultrasensitive terahertz sensing with high-Q Fano resonances in metasurfaces," *Appl. Phys. Lett.* **105**(17), 171101 (2014).
10. M. Gupta, Y. K. Srivastava, M. Manjappa, and R. Singh, "Sensing with toroidal metamaterial," *Appl. Phys. Lett.* **110**(12), 121108 (2017).
11. A. Cui, Z. Liu, J. Li, T. H. Shen, X. Xia, Z. Li, Z. Gong, H. Li, B. Wang, J. Li, H. Yang, W. Li, and C. Gu, "Directly patterned substrate-free plasmonic "nanograting" structures with unusual Fano resonances," *Light Sci. Appl.* **4**(7), e308 (2015).
12. S. Zhang, D. A. Genov, Y. Wang, M. Liu, and X. Zhang, "Plasmon-induced transparency in metamaterials," *Phys. Rev. Lett.* **101**(4), 047401 (2008).
13. Y. Yang, I. I. Kravchenko, D. P. Briggs, and J. Valentine, "All-dielectric metasurface analogue of electromagnetically induced transparency," *Nat. Commun.* **5**, 5753 (2014).
14. S. Yang, X. Xia, Z. Liu, E. Yiwen, Y. Wang, C. Tang, W. Li, J. Li, L. Wang, and C. Gu, "Multispectral plasmon-induced transparency in hyperfine terahertz meta-molecules," *J. Phys. Condens. Matter* **28**(44), 445002 (2016).
15. M. Manjappa, Y. K. Srivastava, and R. Singh, "Lattice-induced transparency in planar metamaterials," *Phys. Rev. B* **94**, 161103 (2016).
16. D. Ö. Güneş, T. Koschny, and C. M. Soukoulis, "Reducing ohmic losses in metamaterials by geometric tailoring," *Phys. Rev. B* **80**(12), 125129 (2009).
17. G. Scalari, C. Maissen, S. Cibella, R. Leoni, and J. Faist, "High quality factor, fully switchable terahertz superconducting metasurface," *Appl. Phys. Lett.* **105**(26), 261104 (2014).
18. V. A. Fedotov, M. Rose, S. L. Prosvirnin, N. Papasimakis, and N. I. Zheludev, "Sharp trapped-mode resonances in planar metamaterials with a broken structural symmetry," *Phys. Rev. Lett.* **99**(14), 147401 (2007).
19. Y. K. Srivastava, M. Manjappa, H. N. S. Krishnamoorthy, and R. Singh, "Accessing the high-Q dark plasmonic Fano resonances in superconductor metasurfaces," *Adv. Opt. Mater.* **4**(11), 1875–1881 (2016).
20. Y. K. Srivastava, M. Manjappa, L. Cong, W. Cao, I. Al-Naib, W. Zhang, and R. Singh, "Ultrahigh-Q Fano resonances in terahertz metasurfaces: strong influence of metallic conductivity at extremely low asymmetry," *Adv. Opt. Mater.* **4**(3), 457–463 (2016).
21. L. Cong, M. Manjappa, N. Xu, I. Al-Naib, W. Zhang, and R. Singh, "Fano resonances in terahertz metasurfaces: a figure of merit optimization," *Adv. Opt. Mater.* **3**(11), 1537–1543 (2015).
22. R. Singh, I. A. Al-Naib, M. Koch, and W. Zhang, "Sharp Fano resonances in THz metamaterials," *Opt. Express* **19**(7), 6312–6319 (2011).
23. C. Jansen, I. Al-Naib, N. Born, and M. Koch, "Terahertz metasurfaces with high Q-factors," *Appl. Phys. Lett.* **98**(5), 051109 (2011).
24. W. Cao, R. Singh, I. A. Al-Naib, M. He, A. J. Taylor, and W. Zhang, "Low-loss ultra-high-Q dark mode plasmonic Fano metamaterials," *Opt. Lett.* **37**(16), 3366–3368 (2012).
25. G. Dayal, X. Y. Chin, C. Soci, and R. Singh, "Independent tailoring of super-radiant and sub-radiant modes in high-Q plasmonic Fano resonant metasurfaces," *Adv. Opt. Mater.* **4**(11), 1860–1866 (2016).
26. M. Manjappa, Y. K. Srivastava, L. Cong, I. Al-Naib, and R. Singh, "Active photoswitching of sharp Fano resonances in THz metadevices," *Adv. Mater.* **29**(3), 1603355 (2017).
27. Y. Moritake, Y. Kanamori, and K. Hane, "Demonstration of sharp multiple Fano resonances in optical metamaterials," *Opt. Express* **24**(9), 9332–9339 (2016).
28. D. R. Chowdhury, X. Su, Y. Zeng, X. Chen, A. J. Taylor, and A. Azad, "Excitation of dark plasmonic modes in symmetry broken terahertz metamaterials," *Opt. Express* **22**(16), 19401–19410 (2014).
29. N. Born, I. Al-Naib, C. Jansen, T. Ozaki, R. Morandotti, and M. Koch, "Excitation of multiple trapped eigenmodes in terahertz metamolecule lattices," *Appl. Phys. Lett.* **104**(10), 101107 (2014).
30. N. Born, I. Al-Naib, C. Jansen, R. Singh, J. V. Moloney, M. Scheller, and M. Koch, "Terahertz metamaterials with ultrahigh angular sensitivity," *Adv. Opt. Mater.* **3**(5), 642–645 (2015).
31. I. Al-Naib, E. Hebestreit, C. Rockstuhl, F. Lederer, D. Christodoulides, T. Ozaki, and R. Morandotti, "Conductive coupling of split ring resonators: a path to THz metamaterials with ultrasharp resonances," *Phys. Rev. Lett.* **112**(18), 183903 (2014).
32. S. N. Burokur, A. Lupu, and A. Lustrac, "Direct dark mode excitation by symmetry matching of a single-particle-based metasurface," *Phys. Rev. B* **91**(3), 035104 (2015).
33. I. Al-Naib, R. Singh, C. Rockstuhl, F. Lederer, S. Delprat, D. Rocheleau, M. Chaker, T. Ozaki, and R. Morandotti, "Excitation of a high-Q subradiant resonance mode in mirrored single-gap asymmetric split ring resonator terahertz metamaterials," *Appl. Phys. Lett.* **101**(7), 071108 (2012).
34. I. Al-Naib, Y. Yang, M. M. Dignam, W. Zhang, and R. Singh, "Ultra-high Q even eigenmode resonance in terahertz metamaterials," *Appl. Phys. Lett.* **106**(1), 011102 (2015).
35. T. Q. Li, H. Liu, T. Li, S. M. Wang, J. X. Cao, Z. H. Zhu, Z. G. Dong, S. N. Zhu, and X. Zhang, "Suppression of radiation loss by hybridization effect in two coupled split-ring resonators," *Phys. Rev. B* **80**(11), 115113 (2009).
36. S. Yang, Z. Liu, X. Xia, Y. e. C. Tang, Y. Wang, J. Li, L. Wang, and C. Gu, "Excitation of ultrasharp trapped-mode resonances in mirror-symmetric metamaterials," *Phys. Rev. B* **93**(23), 235407 (2016).
37. Y. Fan, Z. Wei, H. Li, H. Chen, and C. Soukoulis, "Low-loss and high-Q planar metamaterial with toroidal moment," *Phys. Rev. B* **87**(11), 115417 (2013).
38. M. Gupta, V. Savinov, N. Xu, L. Cong, G. Dayal, S. Wang, W. Zhang, N. I. Zheludev, and R. Singh, "Sharp toroidal resonances in planar terahertz metasurfaces," *Adv. Mater.* **28**(37), 8206–8211 (2016).

39. Z. Liu, S. Du, A. Cui, Z. Li, Y. Fan, S. Chen, W. Li, J. Li, and C. Gu, "High-quality-factor mid-infrared toroidal excitation in folded 3D metamaterials," *Adv. Mater.* **29**(17), 1606298 (2017).
40. M. Gupta and R. Singh, "Toroidal versus Fano resonances in high Q planar THz metamaterials," *Adv. Opt. Mater.* **4**(12), 2119–2125 (2016).
41. A. Tittl, A.-K. U. Michel, M. Schäferling, X. Yin, B. Gholipour, L. Cui, M. Wuttig, T. Taubner, F. Neubrech, and H. Giessen, "A switchable mid-infrared plasmonic perfect absorber with multispectral thermal imaging capability," *Adv. Mater.* **27**(31), 4597–4603 (2015).
42. J. H. Shi, H. F. Ma, W. X. Jiang, and T. J. Cui, "Multiband stereometamaterial-based polarization spectral filter," *Phys. Rev. B* **86**(3), 035103 (2012).
43. C. Zhang, L. Liang, L. Ding, B. Jin, Y. Hou, C. Li, L. Jiang, W. Liu, W. Hu, Y. Lu, L. Kang, W. Xu, J. Chen, and P. Wu, "Label-free measurements on cell apoptosis using a terahertz metamaterial-based biosensor," *Appl. Phys. Lett.* **108**(24), 241105 (2016).
44. G. Dayal, X. Y. Chin, C. Soci, and R. Singh, "High-Q plasmonic Fano resonance for multiband surface-enhanced infrared absorption of molecular vibrational sensing," *Adv. Opt. Mater.* **5**(2), 1600559 (2017).
45. K. V. Sreekanth, Y. Alapan, M. ElKabbash, E. Ilker, M. Hinczewski, U. A. Gurkan, A. De Luca, and G. Strangi, "Extreme sensitivity biosensing platform based on hyperbolic metamaterials," *Nat. Mater.* **15**(6), 621–627 (2016).
46. H. Zhang, C. Li, C. Zhang, X. Zhang, J. Gu, B. Jin, J. Han, and W. Zhang, "Experimental study on the transition of plasmonic resonance modes in double-ring dimers by conductive junctions in the terahertz regime," *Opt. Express* **24**(24), 27415–27422 (2016).
47. W. Liu, S. Chen, Z. Li, H. Cheng, P. Yu, J. Li, and J. Tian, "Realization of broadband cross-polarization conversion in transmission mode in the terahertz region using a single-layer metasurface," *Opt. Lett.* **40**(13), 3185–3188 (2015).
48. N. K. Grady, J. E. Heyes, D. R. Chowdhury, Y. Zeng, M. T. Reiten, A. K. Azad, A. J. Taylor, D. A. R. Dalvit, and H.-T. Chen, "Terahertz metamaterials for linear polarization conversion and anomalous refraction," *Science* **340**(6138), 1304–1307 (2013).
49. J. D. Jackson, *Classical Electrodynamics*, 3rd ed. (Wiley, 1999).
50. N. Papisimakis, V. A. Fedotov, V. Savinov, T. A. Raybould, and N. I. Zheludev, "Electromagnetic toroidal excitations in matter and free space," *Nat. Mater.* **15**(3), 263–271 (2016).

## 1. Introduction

In recent years, metamaterials have attracted tremendous attention due to their exotic electromagnetic properties and functionalities that are not attainable from naturally occurring materials, such as negative refraction [1,2], invisible cloaking [3], subwavelength resolution imaging [4]. The possibility to couple electromagnetic radiation into subwavelength scale makes metamaterials a versatile platform for light manipulation and light-matter interactions. The unique physics observed in metamaterials is generally originated from the resonance nature of their resonant elements. Hence, realizing resonators with high quality (Q) factors is of cardinal importance since various applications require metamaterials that support high-Q-factor resonances accompanying with strong field concentrations in subwavelength volume, such as optical switching [5,6], filtering [7,8], chemical/biological sensing [9–11], and slow light processing [12–15]. However, the Q factor of the majority of metal-based metamaterials is severely limited by high ohmic and radiative losses ( $Q < 10$ ) [13–25], which are considered a major hindrance to the development of typical plasmonic devices. Therefore, demonstration of metamaterials with ultrahigh Q-factor resonances has proven to be a challenging and crucial task for realistic applications.

In general, the ohmic losses at terahertz region are quite low since the noble metals used for fabrication of metamaterials have extremely high conductivity, hence the main challenge in achieving high Q factor resonance in terahertz metamaterials is to ultimately overcome the radiation loss. In order to restrain the radiative loss and reach high Q in metamaterials, several strategies have been proposed and demonstrated by engineering the configuration of the building blocks or controlling the coupling mechanism of the component units. Introducing asymmetry in metamaterials has been proposed as a promising approach to exciting trapped mode or Fano mode with extremely low radiation loss and thus achieving high Q-factor [18–30]. Another approach to remarkably improving Q factor of resonance in metamaterials is to excite dark or sub-radiant modes [31–35], which are usually weakly coupled to free space and cause low radiation loss. The third approach to obtaining high Q-factor resonances is to utilize the diffraction coupling of localized surface plasmon mode in mirror-symmetric

coupled joint split ring resonators, which can trap the photon energy in the subwavelength scale and greatly suppress the radiative loss [36]. In addition, recent studies have reported that high Q-factor resonance can also be achieved if the metamaterial design is tailored in such a way that it could sustain toroidal mode [37–40]. In some planar toroidal metamaterials, the mirroring effect has recently been introduced to support high-Q-factor toroidal dipole mode excitation, whose Q factor is proved to be significantly higher than that of the counterpart Fano resonance [40]. Nevertheless, most of the previous high Q-factor metamaterials only possess single resonance, and excitation of multiple ultrahigh Q-factor resonances may have particular importance for improvement and expansion of functionalities of metamaterials. The ability to integrate multiple and extremely sharp resonances in metamaterial could enable novel designs for multispectral thermal imaging [41], multispectral filters [42], as well as for the realization of advanced label-free bio/chemical sensors [43–45]. The sensing performance of such plasmonic sensors would be greatly benefited from simultaneously detecting the material parameters of the analyte at multiple resonances.

In this paper, we experimentally demonstrate a metamaterial consisting of mirror-symmetry-broken double split ring resonators (MBDSRRs) that sustains double ultrahigh Q-factor resonances with highly suppressed radiation loss. In a conventional mirror-symmetric DSRR array, only the dipole resonance can be excited with the external field perpendicular to the gap of the SRR, and the surface currents are all oriented in phase due to the symmetry constraints. By breaking the symmetry of the mirror-arranged DSRR, we observe the occurrence of two otherwise forbidden ultrahigh-Q-factor resonances with one trapped mode and another octupolar mode. The Q-factor of the trapped mode can be linearly modulated by varying the symmetry parameter of the metamaterial, while the Q-factor of the octupolar mode can be tailored exponentially. This multiple high-Q-factor metamaterial would pave an alternative way to design ultrasensitive chemical and biological sensors, high performance narrow-band filters, absorbers and optoelectronic detectors.

## 2. Metamaterial design and experiment

In the present work, two rectangular SRRs are mirror-arranged to construct mirror-symmetric metamaterial (MDSRR), whereas the mirror-symmetry can be broken by simply shifting one of the SRR gap off the center and thus converted to mirror-symmetry-broken metamaterial (MBDSRR). In this mirrored system, capacitive coupling between the two SRRs is dominated. Therefore, we deliberately employ rectangular SRRs instead of the traditional squared ones to increase the coupling area [46], i.e. increase the capability of field accumulation and reduce radiation loss, and thus enhance the Q factor. Figure 1(a) depicts a schematic of the metamaterial structure with the relevant dimensional parameters and the polarization configuration (the electric ( $E$ ) and magnetic ( $H$ ) fields of the incident wave). The SEM image of the fabricated metamaterial samples is shown in Fig. 1(b). The planar gold MBDSRRs have a side length of  $l_x = l_y = 50.5 \mu\text{m}$ , a width of  $w = 4 \mu\text{m}$ , a mirror distance of  $d = 5.5 \mu\text{m}$ , a gap of  $g = 3 \mu\text{m}$  and super cell lattice constants of  $p = p_x = p_y = 64 \mu\text{m}$ . The asymmetric parameter  $\delta$  is defined as the displacement of the gap of SRR from the central horizontal axis.

The metamaterial samples were fabricated by conventional electron-beam lithography technique, where 200 nm gold structures were deposited on a high-resistivity 1-mm-thick double-side polished silicon ( $n = 3.45$ ) substrate utilizing thermal evaporation and then followed by a lift-off procedure. The overall sample array size is  $5 \text{ mm} \times 5 \text{ mm}$ . The fabricated samples were characterized by broadband terahertz time domain spectroscopy (THz-TDS) system. The terahertz beam had a frequency independent diameter of 3 mm at the focus, which is much smaller than the sample size of  $5 \times 5 \text{ mm}^2$  to prevent beam clipping. The metamaterial samples were placed midway between the transmitter and receiver in the far-field at the focused beam waist, and the transmitted electric field was recorded in the time domain. A bare silicon wafer substrate which identical to the sample substrates, was used as

reference for the transmission measurements. After Fourier transformation of the THz time-domain data, the frequency dependent transmission coefficient of the metamaterials,  $|\tilde{t}(\omega)| = |\tilde{E}_{sam}(\omega) / \tilde{E}_{ref}(\omega)|$ , is obtained from the transmitted THz spectrum of the sample divided by the reference spectrum. All the measurements were performed at a normal incidence with  $x$ -polarization. The experiments were performed at room temperature in a  $N_2$  atmosphere to mitigate the effects of water vapor. Here, a 1-mm-thick high-resistivity silicon substrate was used to delay the Fabry-Perot reflection from the rear surface of the substrate that enabled a scan length of 25 ps with frequency resolution about 40 GHz.

Corresponding numerical simulations were carried out by utilizing commercially full-wave simulation software CST Microwave Studio based on finite integration method. Unit cell boundary conditions in both  $x$  and  $y$  directions along with open boundary condition in the  $z$  direction were applied to the metamaterial unit cell. The simulation parameters of the gold were calculated by the Drude model with plasma frequency  $\omega_p = 1.37 \times 10^{16} \text{ rad s}^{-1}$  and damping rate  $\gamma = 4.08 \times 10^{13} \text{ rad s}^{-1}$  [47,48]. Silicon substrate was modeled as a lossless dielectric with relative electrical permittivity of 11.9.

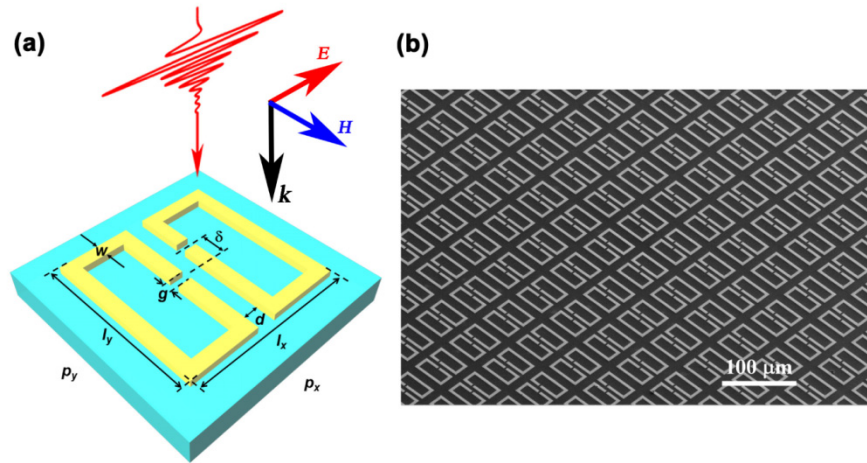


Fig. 1. (a) Structural schematic of the proposed MBDSRR with detailed geometric dimensions. (b) Scanning electron microscopy (SEM) image of fabricated mirror-symmetry-broken metamaterials.

### 3. Results and discussions

Figures 2(a)-2(c) show the SEM images of mirror-symmetric metamaterial (MDSRR), MBDSRR with  $\delta = 8 \mu\text{m}$ , and MBDSRR with  $\delta = 17 \mu\text{m}$ , while the corresponding experimental and simulated transmission spectra of those samples with  $x$ -polarization are shown in Figs. 2(d)-2(f) and Figs. 2(g)-2(i), respectively. Reasonably good agreement is achieved between the simulations and the measurements, and the slightly discrepancies in the frequency and sharpness of the resonances between the theory and the experiments is attributed to the fabrication tolerance and the limited resolution of the THz-TDS system. In the case of MDSRR with the two split gaps at the center of the arms ( $\delta = 0 \mu\text{m}$ ), there is excitation of only one broadband dipolar resonance at 1.16 THz due to the symmetric linear currents oscillating in the two SRR arms parallel to the polarization of the excitation field.

The definition of Q factor is  $Q = 2\pi f_0 \times \frac{P_S}{P_L} = \frac{f_0}{\Delta f}$ , where  $f_0$  is the resonant frequency,  $P_S$  and

$P_L$  are stored and dissipated energy,  $\Delta f$  is the bandwidth at half maxima of the resonance. Thus, the Q factor of the dipolar mode is rather small with a value of 3. Intriguingly, as

gradually breaking the mirror symmetry of the structure by shifting the gap displacement ( $\delta = 8 \mu\text{m}$ ), we observed that two abrupt ultrasharp resonances feature with Q-factor as high as 27 and 37 occur at  $f_1 = 0.45 \text{ THz}$  and  $f_3 = 1.29 \text{ THz}$  in the simulated transmission spectrum, respectively, as shown in Fig. 2(h). The simulated modulation depth  $[(T_{\text{max}} - T_{\text{min}}) \times 100\%]$  for the two resonance are 9.8% and 54%, respectively. The experimentally measured Q factor and modulation depth of  $f_1$  are about 13 and 6.2%, respectively. Relative large deviation in Q factor of  $f_1$  between the simulated and experimental results is due to the rather weak intensity of the resonance as well as the poor spectral resolution at such a low frequency of the THz-TDS system. Besides, the dipolar mode  $f_2$  also appears with the resonant frequency slightly red-shifted. For the sharp resonance  $f_3$ , the corresponding experimentally measured Q factor and modulation depth are 34 and 41.2%, respectively. By further increasing the asymmetry of the MBDSRR ( $\delta = 17 \mu\text{m}$ ), two sharp resonances still appeared and remarkably pronounced with higher modulation depth. From the simulated transmission spectrum, we observed that the modulation depth of  $f_1$  and  $f_3$  increase to 44.5% and 78%, respectively, while the Q factor of  $f_1$  and  $f_3$  decrease to 17 and 25, respectively. The corresponding experimental results indicate that the Q factors for the  $f_1$  and  $f_3$  are 11 and 21, respectively. Meanwhile, the experimental modulation depth of the  $f_1$  and  $f_3$  extracted from the measured spectrum are 28.1% and 55.5%, respectively. It is worth noting that the values of both Q factor and modulation depth of the resonance  $f_1$  and  $f_3$  are much higher than that of the conventional metamaterials (The Q factor of both the fundamental inductive-capacitive and dipolar resonances in conventional metamaterials are usually smaller than ten) [13–23].

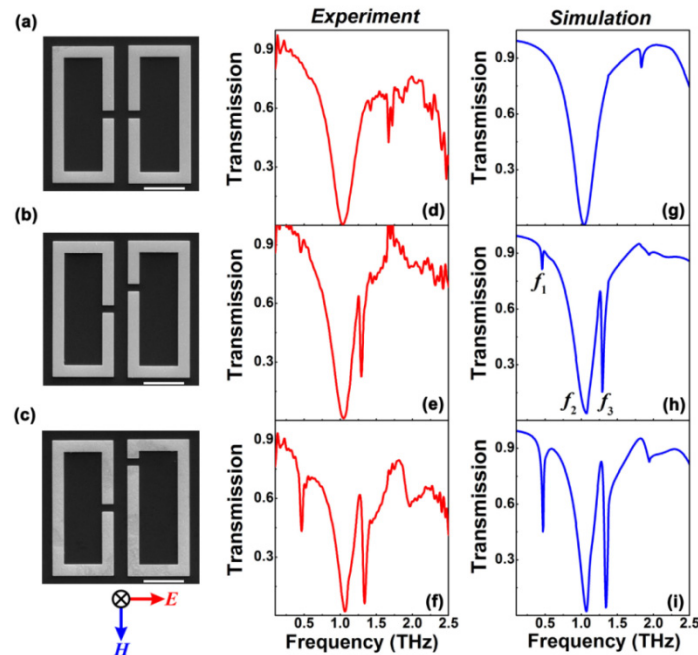


Fig. 2. Scanning electron microscopy (SEM) images of samples (a) MDSRR, (b) MBDSRR with  $\delta = 8 \mu\text{m}$ , and (c) MBDSRR with  $\delta = 17 \mu\text{m}$  are shown in the left column. The scale bar is  $15 \mu\text{m}$ . The measured and simulated transmission spectra of the corresponding the MSRR and MBDSRR structures are shown in the middle and right columns, respectively. Insets depict the incident electric ( $E$ ) and magnetic ( $H$ ) field orientations.

In order to better understand the fundamental nature and physical mechanism of these spectral resonances in greater detail, the surface current and electric field distributions at the three resonant frequencies ( $f_1$ ,  $f_2$ , and  $f_3$ ) were calculated as shown in Fig. 3. The induced surface currents on the MBDSRRs are schematically illustrated by a few electric current

elements, which can be regarded as electric dipoles that radiate electromagnetic waves to the far field. The physical origin of the resonances can be well elucidated by the basic multipole theory in electromagnetic scattering and radiation [36,49]. For the resonance  $f_1$ , two circular electric current loops in the MBDSRR are excited, and the current elements in the SRR arms both along the  $x$  and  $y$  directions always oscillate ( $\pi$ ) out of phase (point in opposite directions) due to the symmetry constraints, such that the electric dipole moment can be well canceled in the direction of the incident field, which dramatically reduces radiative damping and contributes to the formation of the high-Q-factor resonance. In other words, the scatter field for this resonance is dominated by magnetic dipole moment rather than electric dipole moment. According to the aforementioned elaborations, we interpret resonance  $f_1$  as the trapped mode [18] arising from the symmetry breaking inside the structure. In contrast, for the second resonance  $f_2$ , a conventional dipolar resonance is observed, and the surface currents flow in phase along the incident field, which indicate that the radiated electromagnetic fields interfere constructively, as shown in Fig. 3(b). The in phase currents of the dipolar resonance  $f_2$  obviously lead to a comparatively larger net dipole moment than the one induced by the out-of-phase currents in the resonance  $f_1$ , which result in high radiation loss and low Q factor.

For the ultrahigh-Q-factor resonance  $f_3$ , neither a conventional dipole nor a classical trapped mode is observed, but a high-order octupolar mode appeared as depicted in Figs. 3(c) and 3(f). The current and electric field distributions clearly show the characteristic behavior of the  $n = 6$  mode, where  $n$  denotes the eigenmode of the MBDSRR, which manifest that the higher order mode is octupolar in nature [49,50]. The current distributions in the MBDSRR of this particular resonance are of no symmetry, which is distinct from that of the traditional eigenmode of SRRs. Although the current distributions in each SRR behave in a different way, the overall electric current elements in the mirrored SRR also oscillate out of phase, leading to the cancellation of the dipole moment and significant suppression of the radiative loss. What's more, it is worth mentioning that the diffraction coupling effect also plays an important role in the enhancement of Q factor of octupolar mode. According to the diffraction coupling theory [15,36], the resonant frequency of the lattice surface mode is determined by

$$f_{LSM} = \frac{c\sqrt{i^2 + j^2}}{np},$$

where  $c$  is the speed of light in vacuum,  $p$  is the lattice constant of the

metamaterial array,  $n$  is the refractive index of the substrate, and  $(i, j)$  is a pair of integers indicating the order of the lattice surface mode. The resonant frequency of the first order lattice surface mode for our MBDSRR array is 1.36 THz, which is very close to the octupolar mode  $f_3$ . This implies that the photon energy could be strongly confined into the metamaterial structures through diffraction coupling, which dramatically increases the energy stored ( $P_S$ ) by the subwavelength resonators [36]. The current and electric field distributions for  $f_3$  [Figs. 3(c) and 3(f)] clearly show that the ultra-strong localized current and electric fields are confined into the MBDSRR, which manifests that the incident photon energy is strongly trapped into the metamaterials while radiation damping is suppressed, and thus resulting in the ultrahigh-Q-factor octupolar mode.

For the MBDSRR with higher asymmetry ( $\delta = 17 \mu\text{m}$ ), the current distributions for trapped mode  $f_1$  and octupolar mode  $f_3$  are rather similar to those of the MBDSRR with lower asymmetry ( $\delta = 8 \mu\text{m}$ ), and the resonant nature of those modes are not substantially changed. The only change that have taken place is that the current distributions in the left SRR are suppressed while the current distributions in the right asymmetric SRR are enhanced, which leads to a weaker cancellation of the electric dipole moment and huge radiation loss. Therefore, the Q factors of both resonances are degraded as the increase of asymmetry  $\delta$ .

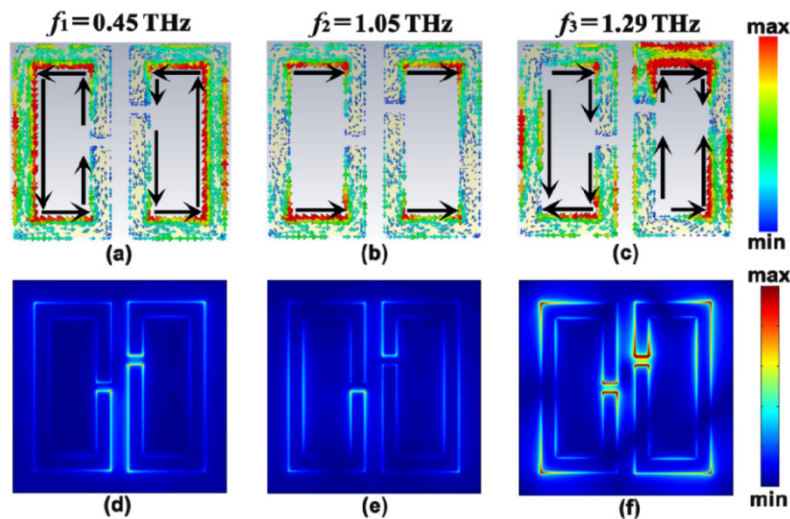


Fig. 3. Surface current and electric distributions for the MBDSRR structure at (a) and (d) trapped-mode resonance  $f_1$ , (b) and (e) dipolar resonance  $f_2$ , (c) and (f) octupolar resonance  $f_3$ . The simulation results of current and electric field intensities are in arbitrary units (color coded). Notice the current and electric field intensities of octupolar resonance  $f_3$  are much larger than those of resonance  $f_1$  and  $f_2$ .

To optimize the Q factor of the metamaterial, we further performed a parametric study of the effect of the asymmetry parameter ( $\delta$ ) on the behavior of the spectral responses. Figure 4(a) depicts the simulated transmission spectra for a sweep of the asymmetry parameter ( $\delta$ ) from 0 to 17  $\mu\text{m}$  by steps of 1  $\mu\text{m}$  each in a color map. All of the resonances  $f_1$ ,  $f_2$ , and  $f_3$  for the MBDSRR exhibit a slight shift towards higher frequencies due to the decreased capacitive coupling in the structure when the asymmetry is increased. Both the trapped and octupolar modes exhibit gradual broadening with an enhancement in the modulation depth as the asymmetry enlarged. The Q factor (left scale) and the modulation depth (right scale) of the trapped and octupolar modes as a function of asymmetry ( $\delta$ ) have also been extracted, as shown in Figs. 4(b) and 4(c), respectively. Although simultaneously maximizing the Q factor and the modulation depth are highly desirable, there exists a significant trade-off between the Q factor and the modulation depth for both resonances. For the trapped-mode resonance  $f_1$ , the Q-factor drastically decreases from 40 to 17 as the asymmetry changes from 1 to 17  $\mu\text{m}$ , while the modulation depth increases rapidly from 0.93% to 44.5% [see Fig. 4(b)]. Increasing the asymmetry results in an enhancement of the modulation depth and a decline of the Q factor approximately in a linear manner. The linear relationship between the Q factor and the degree of asymmetry  $\delta$  is roughly described by  $Q_{f_1} = -K\delta + C$ , where the parameters extracted from the fitted results are  $K = 1.37$  and  $C = 40.6$ , respectively. The Q factor monotonically decreases with higher asymmetry due to the increasing in the radiative loss of the MBDSRR as the difference in the surface current distributions between two excited SRR enlarged and the effective dipole moment are partially canceled in far field.

Interestingly, once introducing the asymmetry parameter  $\delta$  with tiny value (1  $\mu\text{m}$ ), the otherwise forbidden octupolar mode  $f_3$  immediately appeared with extremely high Q nature ( $Q = 106$ ). However, the resonance modulation depth is quite low (5.3%) for such small asymmetry. By further sweeping the asymmetry parameter, an interesting behavior is observed for the octupolar mode. The Q factor exhibits an exponential decreasing behavior versus the asymmetry parameter  $\delta$ , while the modulation depth prominently enhanced from 5.3% to 78.4% when the asymmetry increases [see Fig. 4(c)]. The dependence of Q factor of the octupolar mode on the asymmetry parameter  $\delta$  is summarized as  $Q_{f_3} = A \exp(-\delta/B) + D$

, where the coefficients retrieved from numerical fitting are:  $A = 151$ ,  $B = 3.3$ , and  $D = 23$ , respectively. The decreasing exponential fitting curve reveals the saturation characteristic of the Q factor for the octupolar resonance with large asymmetry ( $\delta > 13$ ). The Q factor decreases exponentially with increasing asymmetry as a consequence of the fact that the cancellation of dipole moment in the MBDSRR is weakened and the remaining net dipole moment causes relative high radiative loss.

Although the physical origin of the degradation of Q factor with increased asymmetry for both modes are similar, the decay manners of the trapped and octupolar modes are quite different due to their distinct resonant nature. The spectral responses of the MBDSRRs strongly depend on the capacitive gap position of the asymmetric SRR, which indicates that the electric (capacitive) coupling in the coupled resonator system is dominant since the magnetic coupling between the resonators is not so sensitive to the gap position of asymmetric SRR. However, it should be noted that the magnetic coupling also plays an important role in the excitation of the sharp trapped mode  $f_1$ , while has less contribution to the dipolar mode  $f_2$  and high-Q-factor octupolar mode  $f_3$ . In addition, it is worth mentioning that both the trapped and octupolar modes are dark modes that are inaccessible in the symmetric configuration, and they only occur when the mirror-symmetry is broken. Once established, varying the asymmetry do not affect the formation of the trapped and octupolar modes, but dramatically tailor the Q factor and modulation depth of those two modes. The MBDSRR possessing double sharp resonances with adjustable Q factor and modulation depth could be used for versatile applications by choosing an appropriate asymmetry parameter.

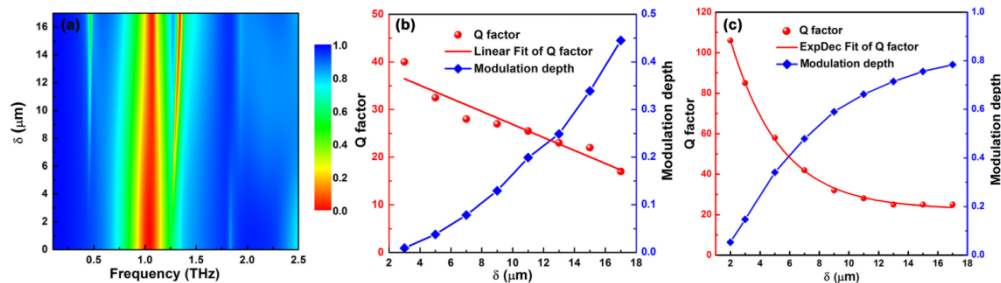


Fig. 4. (a) The transmission spectra of the MBDSRR versus the asymmetry parameter  $\delta$ . The Q factor (left scale) and modulation depth (right scale) achieved of (b) trapped mode  $f_1$  and (c) octupolar mode  $f_3$  when sweeping  $\delta$  for the x-polarization.

#### 4. Conclusions

In conclusion, we experimentally demonstrated a scheme to excite ultrahigh-Q-factor trapped and octupolar modes simultaneously by utilizing metamaterial consists of mirror-symmetry-broken DSRs. By tailoring the asymmetry parameter, both the Q factor and the modulation depth of two resonances could be engineered. When the asymmetry decreased, the Q factor of the trapped mode increases linearly, while the Q factor of the octupolar mode increases exponentially. Moreover, the mirror-symmetric-broken metamaterials with multipole high-Q-factor resonances could be extremely useful in real world applications such as spectroscopy, communications, nonlinear optics, and coherent lasing spasers.

#### Funding

National Key Research and Development Program of China (Grant Nos. 2016YFA0200400, and 2016YFA0200800); National Natural Science Foundation of China (Grant Nos. 91323304, 11674387, 11504414, 11574369, 11574385, 11574368, 61390503); Strategic Priority Research Program of the Chinese Academy of Sciences (Grant No. XDB07020200).